ACS OMEGA

http://pubs.acs.org/journal/acsodf

Article

Facile Synthesis of Barium-Doped Cadmium Sulfide Quantum Dots for the Treatment of Polluted Water: Experimental and Computational Investigations

Ata Ur Rehman, Muhammad Ikram,* Ali Haider, Muhammad Asif Raza, Tahira Shujah, Misbah Naz, Anwar Ul-Hamid, Iram Shahzadi, Souraya Goumri-Said, Mohammed Benali Kanoun, and Walid Nabgan*

Cite This: *ACS Omega* 2022, 7, 46325−46336

Read Online

ACCESS | Metrics & More | Article Recommendations | Supporting Information

ABSTRACT: In this study, cadmium sulfide (CdS) quantum dots (QDs) and barium (Ba) (3 and 6 wt %)-doped CdS QDs were synthesized via a hydrothermal technique. The basic purpose of this work is to degrade methylene blue (MB) dye and evaluate density functional theory (DFT). The synthesized samples were characterized through X-ray powder diffraction (XRD), selected area electron diffraction (SAED), Fourier transform infrared spectroscopy (FTIR), scanning electron microscope (SEM), high-resolution transmission electron microscopy (HR-TEM), UV−vis spectrophotometer, PL, and density functional theory (DFT). The XRD (structural analysis) confirmed that the hexagonal crystal structure and crystallinity increased upon doping. Selected area electron diffraction (SAED) analysis confirmed the polycrystalline nature of the prepared QDs. The functional groups have been investigated using FTIR analysis. The surface and structural morphologies of the synthesized specimen have been investigated by applying TEM and FE-SEM, and it was found to exhibit the topology of QDs. In addition, optical characteristics have been investigated via UV−vis absorption spectroscopy, which exhibited a bathochromic shift (red shift) as a consequence of the reduction of the band-gap energy upon doping from 2.56 to 2.38 eV. PL analysis was used to observe the electron−hole recombination rate. Moreover, the electronic and optical properties of Ba-doped CdS were further explored using density functional theory. Pristine and Ba-doped QDs exhibit sufficient catalytic activity (CA) against the MB dye in all media as 62.59, 70.15, and 72.74% in neutral, basic, and acidic solutions, respectively.

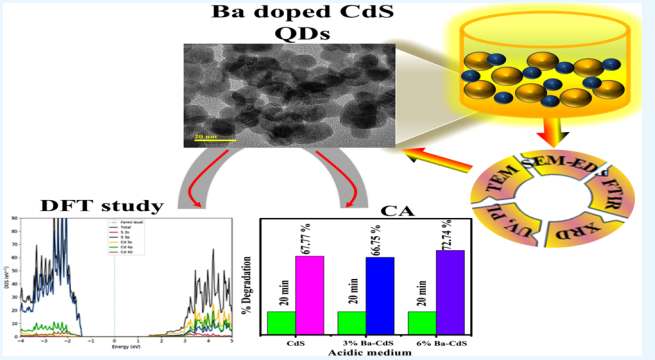

1. INTRODUCTION

Water pollution has become a major issue with increasing population growth. A large amount of industrial waste is disposed of directly in water resources without purification.[1] Water resources get contaminated with dyes and phenolic compounds harmful to the environment, and they are difficult to degrade via natural phenomena.[2] Annually, 1×10^6 to 10^7 ton dyes are produced in various industries such as rubber, paper, pigment, paint, printing, plastic, textile, and leather.[3,4] Approximately 10−15% of industrial dyes are directly discharged into freshwater resources and the surrounding environment, causing critical diseases in humans.[5] Moreover, methylene blue (MB)-contaminated water causes many harmful issues in aquatic life.[6] These dyes are highly soluble in water; both mutagenic and poisonous effects are caused by a substance with high stability to light, which can disrupt the transmission of sunlight into water.[7] Wastewater treatment for removing toxic dyes poses a big problem for protecting the environment and human health.[8] Various techniques, including transition-metal sulfides,[9,10] metal oxides,[9,11] chemical precipitation, conventional coagulation, electrodeposition, filtration, electrolysis, ion exchange, adsorption catalysis, and photocatalysis degradation, have been applied to wastewater treatment for the removal of dyes. These techniques are either slow or nondestructive to some persistent organic pollutants and have limitations in large-scale implementation.[12] Catalytic degradation has been used for the degradation of various dyes because it is environment-friendly, cost-effective, and efficient.[13] The use of semiconductor catalysts is favored in dye degradation due to the fact that it is a sustainable and environmentally friendly method for wastewater treatment.[14]

Received: August 1, 2022
Accepted: November 24, 2022
Published: December 9, 2022

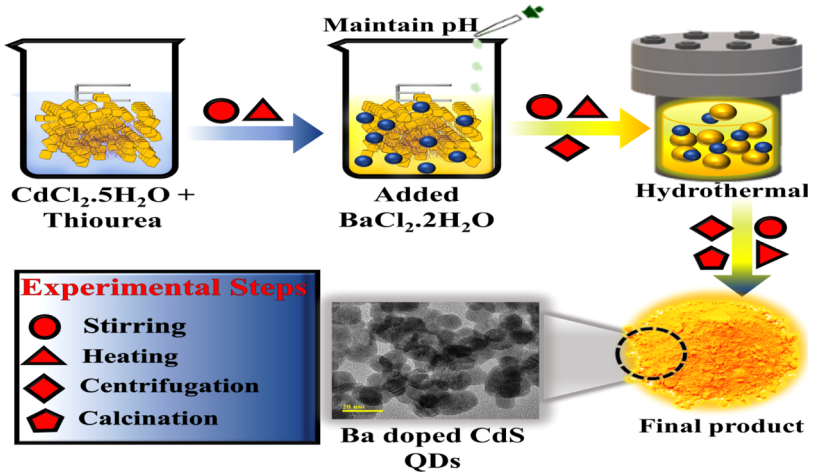

Figure 1. Schematic diagram of CdS quantum dot-doped Ba.

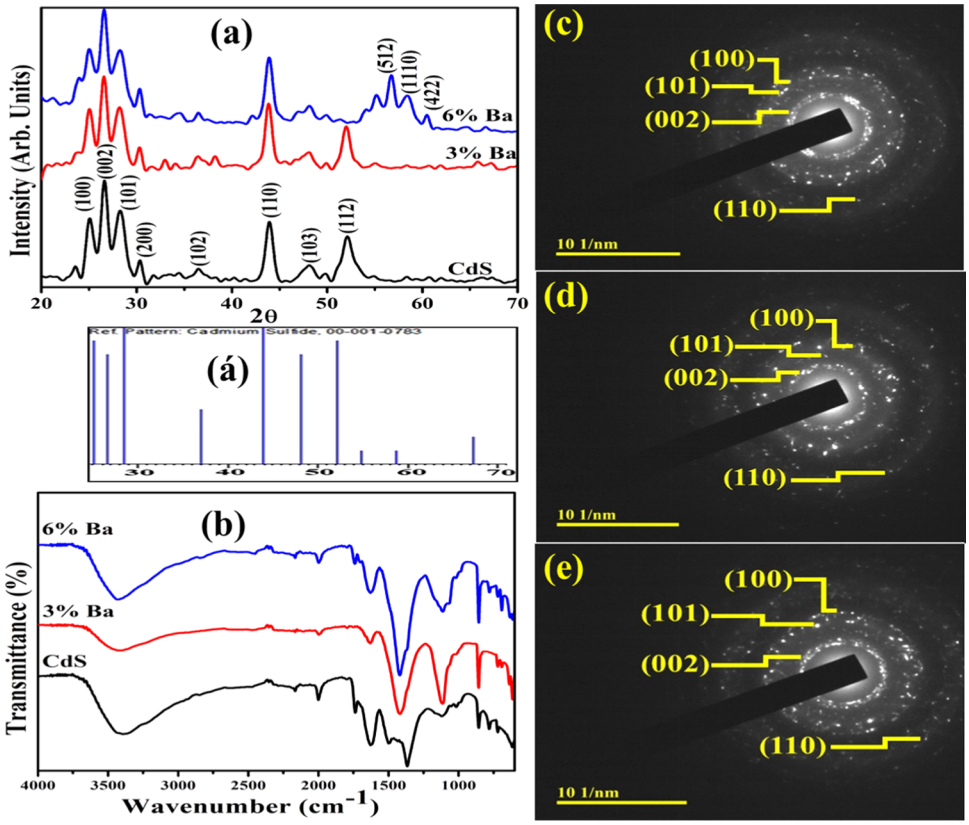

Figure 2. (a) XRD pattern of synthesized doped CdS. (b) FTIR spectra (c−e) and selected area electron diffraction (SAED) pattern of CdS, 3 and 6% Ba-doped CdS.

Several catalysts have been synthesized, such as transition-metal oxides,[11,15,16] metal sulfides,[10,17] composite structures,[18,19] and dopant materials,[13,18,20] to improve the efficiency of degradation. Synthesis of low-cost and high-activity catalysts for removal of toxic dyes is still a challenge.[21] Metal sulfides such as cadmium sulfide (CdS), which has an ideal band gap of 2.42 eV, can function as a potential catalyst for the reaction.[22] CdS has unique properties, including decomposition of toxic organic compounds and resistance to optical and chemical corrosion,[23] as well as detection of visible radiation and conduction band.[24,25] Because CdS has only a few surface trapping states, it works well in electrical and optical applications. The fluorescent semiconducting colloidal crystals are known as CdS QDs. With their exceptional optical and electrical characteristics, CdS NPs or QDs can be used in a variety of applications.[26,27] It exists in three crystalline phases: wurtzite, zinc blende, and high-pressure rock salt.[28] CdS has been used in many applications such as in solar cells,[29] photodetectors,[30] gas sensors,[31] and antibacterial activities[32] as well as in catalytic degradation of dyes.

CdS has a high capacity for degradation; however, this capacity is contingent on its interaction with an appropriate dopant material. Transition-metal (Mn, Co, Ti, Ba, etc.)-doped CdS showed optical, electrical, and magnetic properties.[21,33] Ba

https://doi.org/10.1021/acsomega.2c04862
ACS Omega 2022, 7, 46325−46336

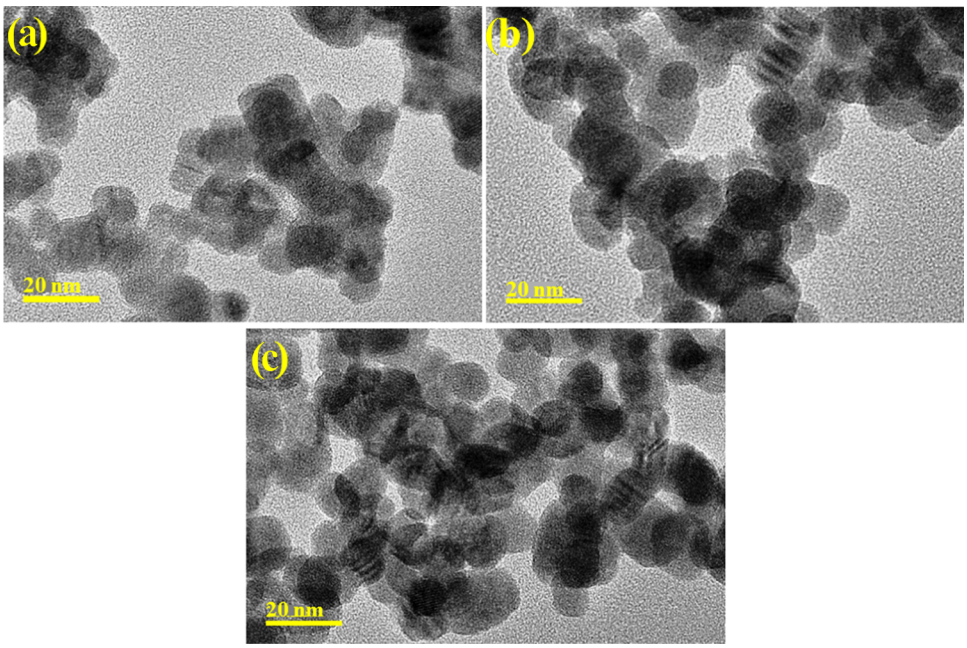

Figure 3. TEM images of (a) pristine CdS, (b) 3% Ba-doped CdS QDs, and (c) 6% Ba-doped CdS QDs.

doping in CdS offers potential electrical, optical, and magnetic properties. The nanoparticle was synthesized using various methods, including chemical coprecipitation, sol−gel, and hydrothermal methods. The hydrothermal method was used because it is environment-friendly, economical, had easy-to-prepare required material, and milder.[34]

In this work, pristine and Ba (3 and 6%)-doped CdS quantum dots (QDs) have been effectively synthesized via a hydrothermal approach. The synthesized QDs have been employed to remove the toxic MB dye. A number of characterization techniques have been used to investigate the detailed analysis of the prepared QDs. Also, we looked into the Ba-doped CdS surface using density functional theory calculations. We demonstrate that the changes in the electronic structure of Ba doping into the CdS surface can be explained by combining experimental findings with theoretical calculations.

2. EXPERIMENTAL SECTION

2.1. Materials. Cadmium chloride 2,5 hydrate ($CdCl_2$. $5H_2O$, 99%) was obtained from PRS Panreac (Barcelona). Thiourea (NH_2CSNH_2, >99%) as the sulfide source, ammonia solution (max. 33% NH_3), and barium chloride dihydrate ($BaCl_2.2H_2O$, >99%) were procured from Sigma-Aldrich (Germany).

2.2. Synthesis of Ba-Doped CdS. The hydrothermal technique was adopted to synthesize CdS and Ba-doped CdS quantum dots (QDs). A 0.2 M solution of $CdCl_2$, $5H_2O$, and NH_2CSNH_2 was prepared under continuous heating and stirring at 80 °C for 30 min. Then, 0.5 M NaOH was poured dropwise to maintain the pH ∼ 12 and the formation of precipitates. The required amount of ammonia was added to obtain a yellowish precipitate. The solution was kept in an autoclave at 150 °C for 24 h, and yellowish precipitates were washed with DI water using centrifugation at 7500 rpm and the synthesized sample was dried at 150 °C overnight. Different concentrations of Ba (3 and 6%) as a doped material were incorporated in the CdS solution using the above-mentioned method to obtain Ba-doped CdS fine powder, as indicated in Figure 1.

3. RESULTS AND DISCUSSION

XRD diffraction analysis was used to confirm the chemical composition, crystallographic structure, and crystalline size of the synthesized undoped and Ba-doped samples, as represented in Figure 2a. The hexagonal structure of the prepared sample has been exhibited in JCPDS card no. 00−001−0783. Figure 2á shows the JCPDS card matched with the obtained XRD data. The diffraction peaks observed at 2θ are 25.10, 26.62, 28.29, 30.40, 36.40, 43.93, 48.21, and 52.21°, which correspond to (100), (002), (101), (200), (102), (110), (103), and (112) planes. The strongest peak was observed at an angle of 26.62° with the (002) plane, as described by several other researchers.[35] The peak observed at 36.43° showed a hexagonal structure of the pure sample, which corresponds to JCPDS card no. 01-075-0581, and the one at 30.37° has been well matched with JCPDS card no. 01-075-0581, demonstrating a cubic crystal structure. The crystallite size was measured with the Debye−Scherrer formula of pure CdS is 20.73 nm, which drops to 17.27 nm for 3% Ba-doped and increases to 18.73 nm for 6% Ba doped. A similar crystalline size variation was observed in previously reported results.[36] Compared to pure CdS, the 6% Ba-doped CdS peak position at the angle 58.38° slightly shifted toward a high angle and extra peaks were observed at angles 56.79 and 60.42°, matching with JCPDS card no. 01-079-1644. Peak shifting was detected due to variation of the ionic size of the host and the dopant material, as induced by compressional and tensile stress and the thermal expansion of the dopant and host ions in the XRD pattern.

Fourier transmission infrared spectroscopy has been used to search for the presence of various functional groups and the chemical composition of host and Ba-doped CdS QDs in the range of 4000−500 cm^{-1} (Figure 2b). The sharp absorption band at 3410 cm^{-1} was linked with the O−H stretching vibration of a water molecule that was absorbed on the surface of pristine and doped CdS QDs. The weak band detected at

https://doi.org/10.1021/acsomega.2c04862
ACS Omega 2022, 7, 46325−46336

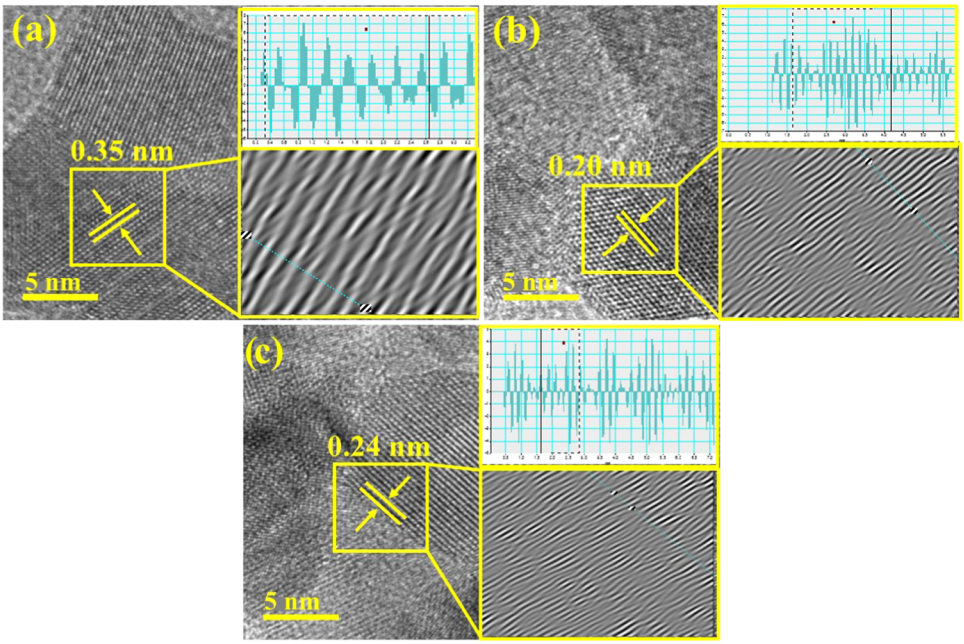

Figure 4. Interlayer *d*-spacing of (a) pristine CdS, (b) 3% Ba-doped CdS QDs, and (c) 6% Ba-doped CdS QDs.

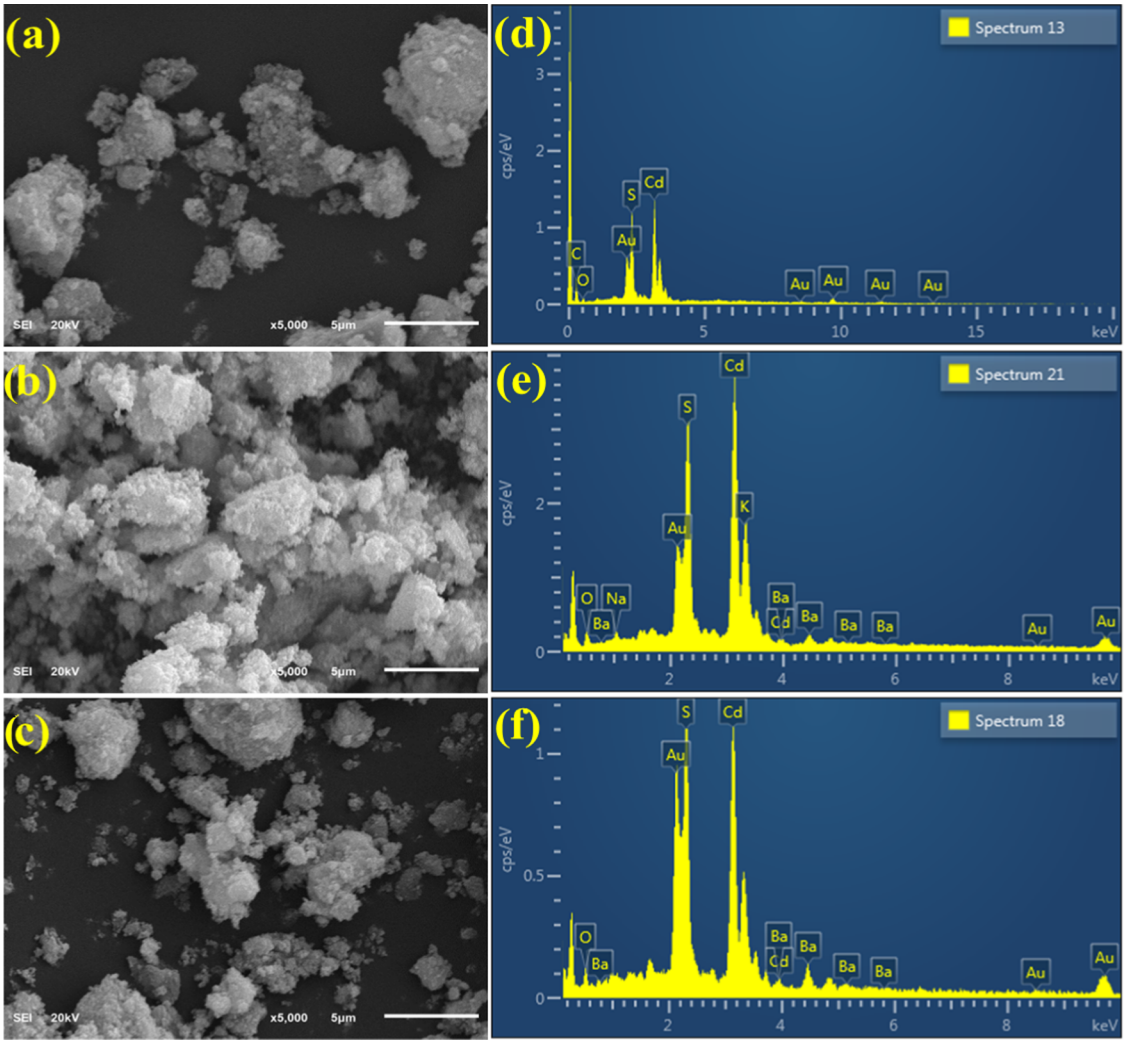

Figure 5. Elemental compositions and surface morphologies of CdS and 3 and 6% Ba-doped CdS (a–c). FE-SEM images and (d–f) EDS analysis.

https://doi.org/10.1021/acsomega.2c04862
ACS Omega 2022, 7, 46325−46336

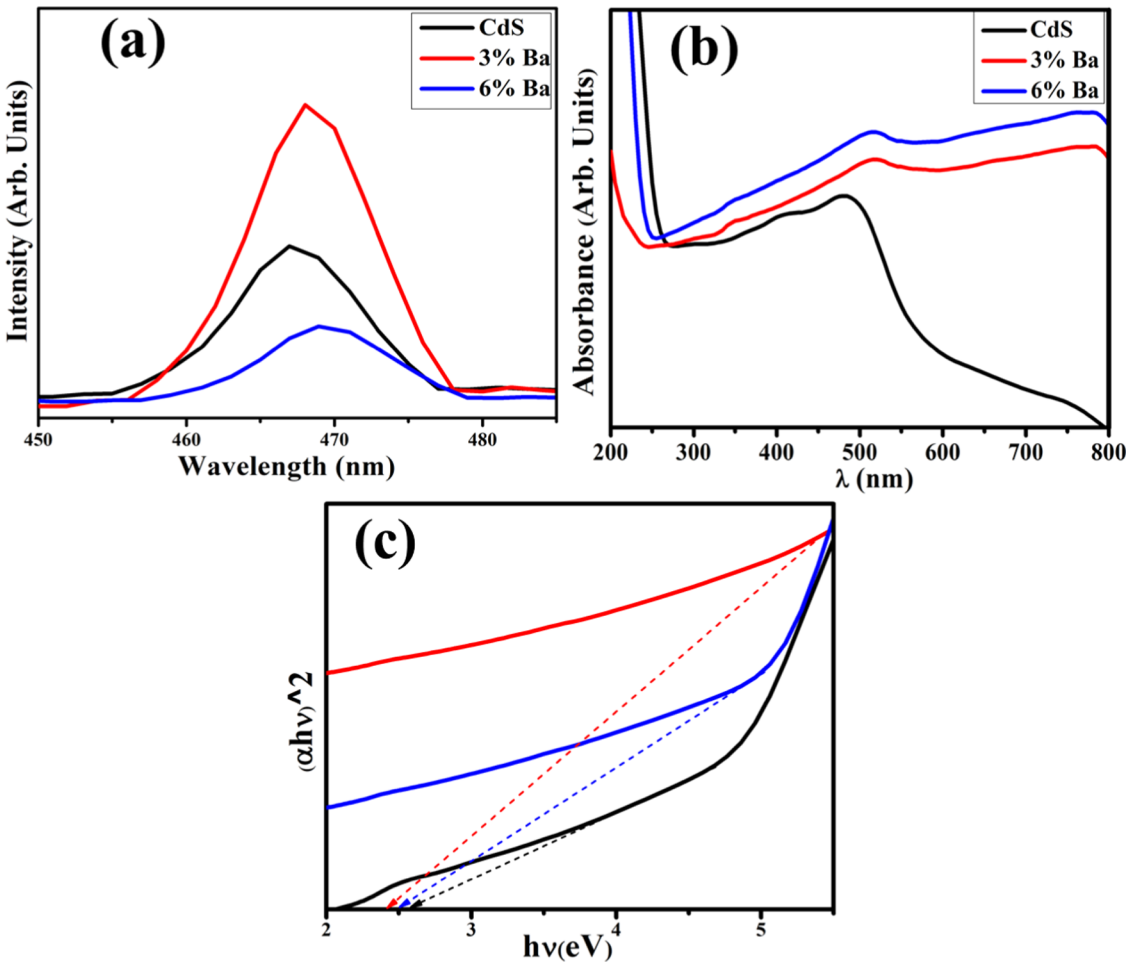

Figure 6. Optical analysis of synthesized pure and 3 and 6% Ba-doped CdS QDs (a), PL spectra (b), and band-gap energy plot (c).

1625 cm^{-1} exhibited the bending vibration of O−H, confirming the presence of water molecules due to moisture.[37] The spectra showed a band at 2158 cm^{-1}, demonstrating the stretching vibration of the −OH bond, which indicates the strong interaction of CdS with water molecules.[38] The observed bands at 1736, 1490, and 856 cm^{-1} have been attributed to the stretching vibration of the C═O bond, the CH_3 antisymmetric vibration, and the CH_2 vibration, respectively[33,39] The CH_3 and CH_2 vibrations are observed due to the use of thiourea and ammonia solution during the synthesis process. The stretching vibration of the sulfide group is connected with the wide band that may be seen at 1368 cm^{-1}. The band appeared at 1123 and 1017 cm^{-1} and has been assigned to the SO^{4-} group. The absorption band appears at 720 and 618 cm^{-1}, which can be attributed to Cd−S stretching.[40] The spectra of pristine and doped samples showed that all spectra exhibit the same feature. Results show that increasing the dopant concentration bands of O−H, C═O, CH_3, and CH_2 decreased the intensity, with the peak shifting toward lower wavenumbers. This phenomenon indicates the coordination between host and dopant ions. SAED analysis has been used to confirm the prepared single-crystalline or polycrystalline specimens and observe only the position of the diffracted beam. The synthesized sample indicates bright circular rings of CdS and Ba-doped CdS QDs that are polycrystalline, as indicated in Figure 2c−e. The results of XRD measurements that satisfy Bragg's diffraction conditions are well matched with the various planes of the synthesized QDs.

Transmission electron microscopy (TEM) analysis has been employed to confirm the structural morphology of undoped and Ba (3 and 6%)-doped CdS (Figure 3a−c). The CdS morphology has cubic and spherical quantum dots, as represented in Figure 3a. Upon various concentrations of Ba (3 and 6%) doping, the particle exhibited aggregation and agglomeration of quantum dots and a rodlike morphology appeared, as can be seen in Figure 3b−c. High-resolution TEM (HR-TEM) image with 5 nm resolution was used to find the interlayer d-spacing. The measured d-spacing of pure and Ba (3 and 6%)-doped CdS was measured using Gatan software and was found to be 0.35, 0.20, and 0.24 nm, respectively. The measured interlayer *d*-spacing is confirmed by XRD measurement, as revealed in Figure 4a−c.

Scanning electron microscope (SEM) analysis was used to exhibit the surface morphology of pure and Ba-doped CdS depicting a nonhomogeneous cluster structure, as illustrated in Figure 5a−c. The low- and high-magnification images of a pure sample have been shown, as in Figure S1. Upon doping Ba 3%, the cluster size increased, so a high degree of agglomeration of quantum dots was observed. The particle size increases upon increasing the Ba concentration by 6%, with a small agglomeration observed. On increasing the cluster size, the agglomeration decreased, and vice versa.[41]

https://doi.org/10.1021/acsomega.2c04862
ACS Omega 2022, 7, 46325−46336

The elemental composition evaluated by energy-dispersive X-ray spectroscopy (EDS) confirms the successful formation of CdS, as represented in Figure 5d−f. Ba-doped EDS spectra at various concentrations (3 and 6%) confirmed the successful doping of Ba in CdS. Additional peaks of Na have been observed because of added NaOH to maintain the pH and observe the precipitates, while additional Au has been attributed to a sputtering-coating of Au to cover charge dissipation.[42]

Photoluminescence (PL) analysis was employed to obtain the information based on impurities, derive the transitions of the energy state, and study the emission spectra of dopants, as indicated in Figure 6a. The PL spectra of host and Ba-doped CdS QDs have been measured in the range of 370−500 nm to elucidate the electron−hole pair recombination process. The emission peak observed at 466 nm due to luminescence originated from sulfur vacancies.[43] The PL emission intensity is directly related to electron−hole recombination, although a higher recombination rate shows fluorescence and the lowest peak intensity observed from phosphorescence. The PL spectra exhibited a slight red shift upon doping of Ba, which correlates with the absorption spectra, as shown in Figure 6a. Upon Ba (3%) doping, a higher peak intensity was noted on increasing the concentration (6%) of Ba, which reduced the peak intensity owing to a lower recombination rate. The decrease in PL intensity was because of the different energy states.[44]

Optical properties of pristine and Ba-doped CdS QDs were studied using UV−vis spectrophotometry in the range of 200−800 nm in Figure 6b. The absorption peak of pure CdS QDs was observed at 483 nm.[45] Using Tauc's equation to calculate the band-gap energy (E_g), the direct E_g was found to be 2.56 eV, which is consistent with previously reported findings.[46,47] Incorporating various concentrations of Ba into pristine samples indicates that the absorption spectra have shifted toward a higher wavelength (red shift). The red shift in absorption peak has been associated with the decrease in carrier concentration by incorporation of the doped material and a decrease in the band-gap energy. The ionic radius of Ba^{+2} ions is higher than the pristine exhibit of the red shift.[15] The decrease in band gap ascertained the interaction among s, p, and d suborbitals of the shell. The d-subshell energy of the Ba^{+2} ion is almost close to the s-subshell of the same ion.[41]

The structural and optoelectronic characteristics of Ba-doped CdS were further clarified using first-principles computation. Our calculations were performed using the first-principles software package QuantumATK[48] based on density functional theory (DFT). The Perdew−Burke−Ernzerhof (PBE) functional[49] under the generalized gradient approximation (GGA) was used to characterize the exchange and correlation potentials. A Monkhorst−Pack *k*-point grid of 6 × 11 × 1 was employed in the calculation. To fully optimize the structural geometry, the convergence accuracy of the residual force during relaxation was set to less than 0.05 eV/Å for each atom. The electronic structure was calculated by DFT using the HSE06 functional.[50,51] The CdS surface is constructed from the primitive cell of bulk CdS. The calculated lattice parameters of the bulk hexagonal CdS ($a = b = 4.139$ Å and $c = 6.733$ Å) agree well with the experimental results ($a = b = 4119$ Å, $c = 6.7264$ Å).[52] The CdS surface is modeled by a (1 × 2) 7-layer supercell along the $11-19$ direction having a hexagonal structure containing a total of 56 formula units, as shown in Figure 7. A vacuum region of 15 Å separated each slab from one another along the (11−20) direction.[53] To

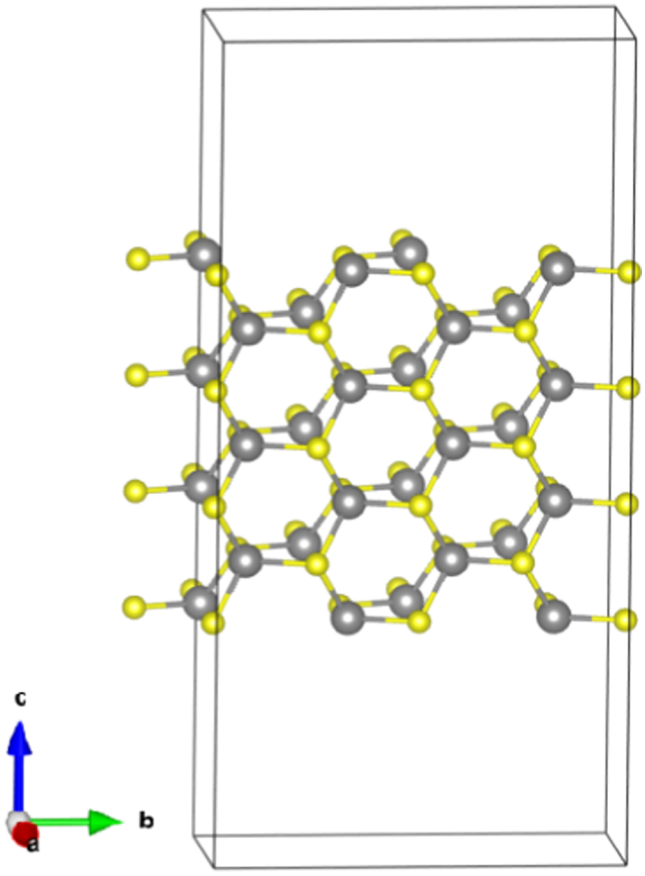

Figure 7. Schematic of the (11−20) surface slab model with seven CdS layers; the gray and yellow balls denote the Cd and S atoms, respectively.

explore the influence of the Ba-doping system, single and two Ba atoms are introduced into the slab at Cd substitutional positions on the surface slab, which correspond to total dopings of 3.57 and 7.1%, respectively. The electronic structure of Ba near the (11−20) surface is investigated, where the densities of states (DOS) are computed and shown in Figure 8 for different concentrations. As shown in Figure 8a, HSE06 calculation results of the DOS plot and the band structure (not shown here) for the pure CdS surface with the band structure reported in previous theoretical works[54] can be found in the form of a direct band gap at the Γ-point. It is observed that the highest occupied state of the CdS surface is mainly derived from the S 3s states, while the lowest unoccupied state is generated from the Cd 5s and Cd 4p states. A significant optical band gap results from the principal optical absorption occurring below the edge of the valence band. Thus, the CdS surface indicates a band-gap value of 2.83 eV, which is consistent with the experimental results of 2.55−2.65 eV.[55] As illustrated in Figure 10, the band gap decreased to 2.76 and 2.67 eV with the increase of the Ba concentrations for 3.57 and 7.1%, respectively, which leads to a small downshift to the lowest part of the conductor band and a small upshift to the highest part of the valence band. We computed the absorption coefficient spectra using the HSE06 functional, as shown in Figure 8, to investigate the absorption features in the pure and Ba-doped CdS surface. The examination of the absorption coefficients revealed that the pure CdS surface could absorb in the visible range. The impurity in the gap state

https://doi.org/10.1021/acsomega.2c04862
ACS Omega 2022, 7, 46325−46336

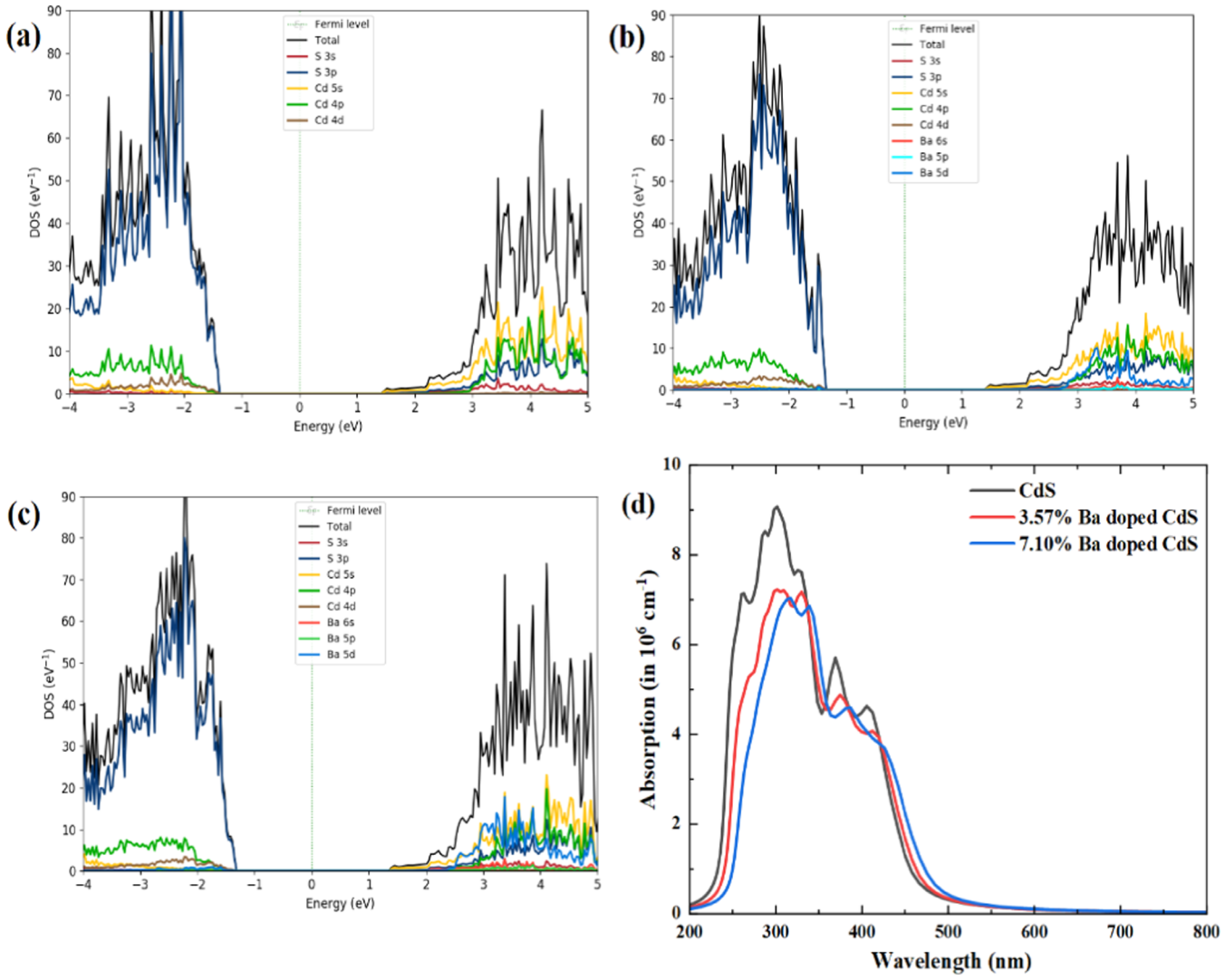

Figure 8. Calculated total and partial DOS of (a) pure, (b) 3.57%, and (c) 7.1% Ba-doped CdS surface, and (d) optical absorption spectra.

caused a minor red shift of the absorption edge as a result of the Ba doping.

With 400 L of $NaBH_4$ serving as the reducing agent and 3 mL of freshly made MB solution (10 ppm) serving as the oxidizing agent, the CA of pure and Ba-doped CdS QDs was conducted. As a result, 400 mL of synthetic CdS QDs and CdS QDs doped with Ba (3 and 6%) were added to the initial solution. The degree of dye absorption revealed the decolonization rate at a certain time. A UV−vis spectrophotometer was used to study the degradation rate, and the percentage degradation was measured as follows:

$$\% \text{ degradation} = ((C_o - C_t)/C_o) \times 100$$

where dye concentrations at initial and specific times are C_o and C_t, respectively.

Catalysts, in general, speed up reactions in ongoing experiments; however, choosing a larger or lower amount of catalyst than necessary can slow down a reaction. Therefore, using the right amount of catalyst is crucial for a dye degradation experiment to succeed. During catalysis, a reducing agent ($NaBH_4$) provides an e^- to MB, as an oxidizing agent. The transfer of e^- from $NaBH_4$ to MB is a redox reaction that occurs during CA, resulting in the degradation of the synthetic dye, as shown in Figure 9. In the absence of a nanocatalyst, the process is very slow. The rate

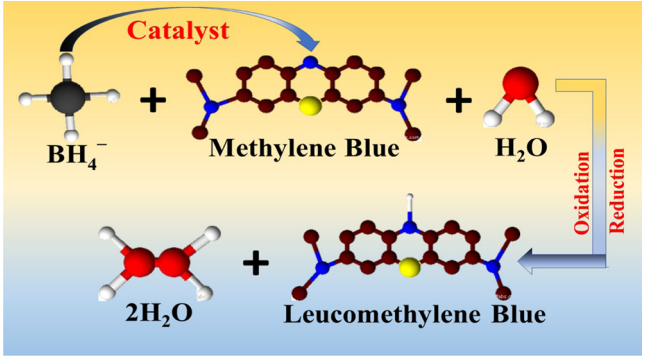

Figure 9. Degradation mechanism of MB dye.

of the reaction increases after the addition of a nanocatalyst (CdS and doped QDs). Catalysts lower the activation energy (E_a) of a reaction, which in turn stabilizes and enhances the reaction rate.[56]

The degree of degradation is influenced by the pH of solutions, and dye effluents are frequently released at different

https://doi.org/10.1021/acsomega.2c04862
ACS Omega 2022, 7, 46325−46336

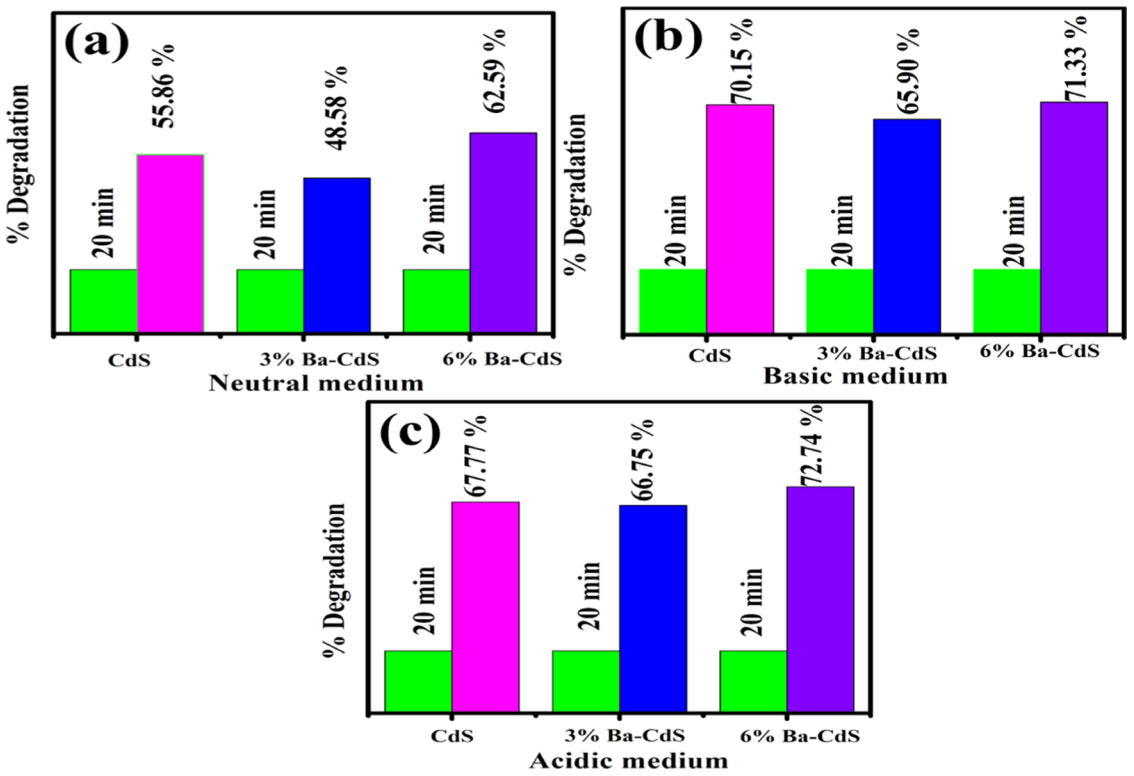

Figure 10. % Degradation of synthesized QDs: (a) neutral medium, (b) basic medium, and (c) acidic medium.

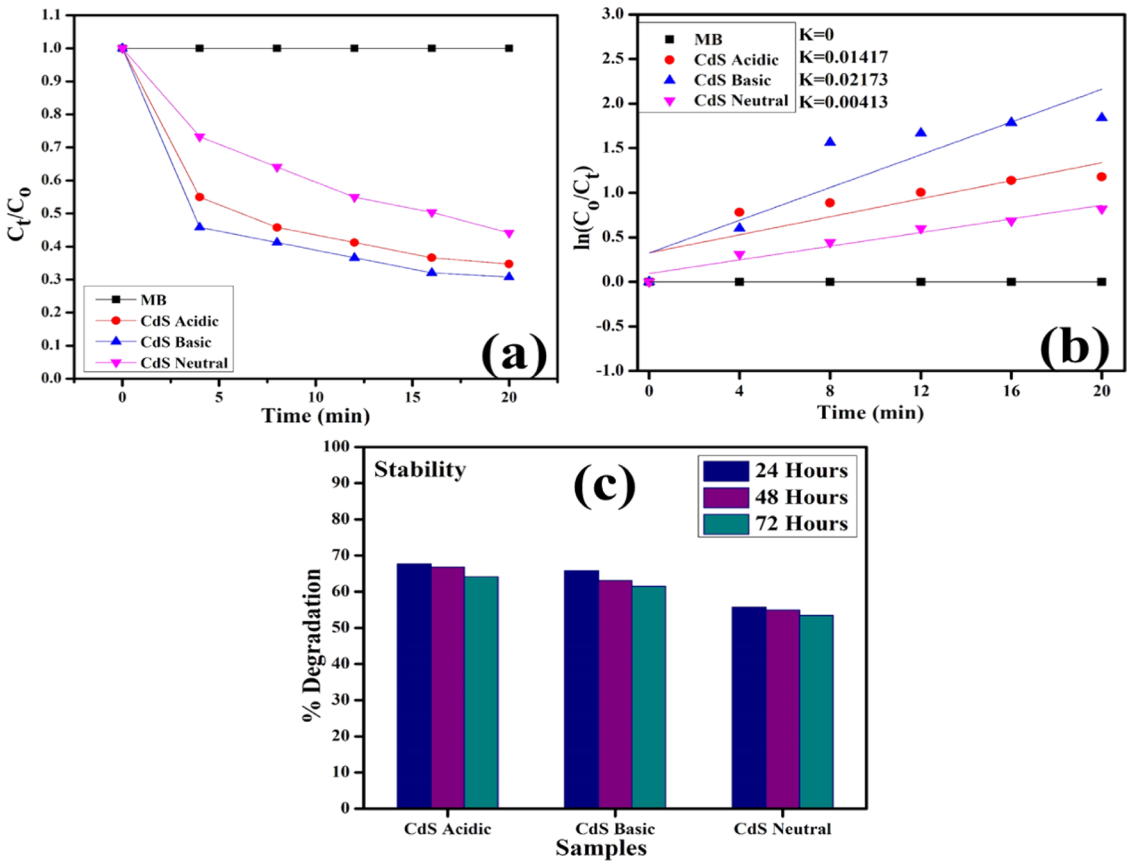

Figure 11. (a) Plot of the concentration ratio (C_t/C_0) versus time for CdS. (b) Plot of $\ln(C_0/C_t)$ versus time spectra of CdS. (c) Stability of the pure catalyst CdS.

https://doi.org/10.1021/acsomega.2c04862
ACS Omega 2022, 7, 46325−46336

Table 1. Comparison of the Catalytic Activity of the Synthesized QDs with the Present Study

nanocatalyst	synthesis route	% degradation	activity	outcomes	refs
TM-doped CdS	Coprecipitation route		catalytic activity	Ni- & Co-doped CdS showed maximum degradation	21
Fe-CdS	Coprecipitation	100	catalytic activity	15% Fe-CdS degraded MB dye 100% in 10 min	62
CNC-g-PVP-doped CdS QDs	Coprecipitation	99.79	catalytic activity	at 8 min, degradation was about 99.79%	60
Ba-doped CdS QDs	hydrothermal method	72.74	catalytic activity	6% Ba-CdS showed maximum degradation 72.74%	present work

pH levels.[57] The surface charge of dye molecules and catalysts is strongly influenced by the pH of the solution. Positively charged catalyst surfaces fight against cationic species adsorption in an acidic medium. Due to the powerful electrostatic interaction between the negatively charged catalyst and the negatively charged cationic dye in the basic media, the surface becomes negatively charged. Multiple morphologies are observed after doping that give more active sites for charge transfer. QDs have a large surface area and crystallinity, describing more charge transfer. The reducing capacity of $NaBH_4$ was also studied in the absence of catalysts.[58] However, low degradation was observed after 20 min due to the small catalytic activity of $NaBH_4$. The prepared nanocatalyst (400 μL) was added to the solution, increasing the dye degradation. The catalytic material acts as an electron relay, and the transportation of electrons from BH_4^- to the MB results in degradation of the dye. In the oxidation−reduction reaction, the catalyst enhanced the reaction rate by lowering the activation energy and providing large nanocatalyst sites.[59] The presence of a nanocatalyst and a reducing agent improves the dye degradation efficiency; the mechanism is represented in Figure 9.

The pure and Ba (3 and 6%)-doped CdS QDs exhibit degradations of 55.86, 48.58, and 62.59% in neutral; 67.77, 66.75, and 72.74% in acidic; and 70.15, 65.90, and 71.33%, in basic mediums, respectively, within 20 min, as represented in Figure 10a−c. The absorption spectra that demonstrate the reduction of the MB dye in an acidic medium have been shown in Figure S2. The degradation was affected by the pH of the solution, crystallinity, morphology, and surface area of QDs.

Catalytic activity increased in an acidic medium, which can be associated with the increased production of H+ ions adsorbed on the surface of the quantum dots.[60] The improvement in catalytic effectiveness for both acidic and basic mediums observed in this study has been attributed to the size and morphology of QDs acting as catalytic agents.[61] The maximum degradation of MB has been observed in a basic medium because with the addition of NaOH to make the dye solution basic, the surface of the catalyst becomes negatively charged and MB is positively charged. The electrostatic attraction between the dye and the surface of the catalyst increases the adsorption rate and results in dye degradation. At low pH ∼ 4 (acidic medium), the surface of the catalyst becomes positively charged and the MB is also positively charged; the electrostatic repulsion between positive and negative charges decreases the adsorption, which results in less degradation in an acidic medium for pure and 3% Ba doping. On increasing the doping concentration (6%), the maximum degradation was noted, which increased the number of H^+ in the dye solution to degrade at a maximum of 72.74%.

The nanocatalysts considerably enhance the catalytic degradation of MB and efficiently destroy the dye (Figure 11a). The large surface area of CdS QDs resulted in an enhanced catalytic activity. Rate constants (k) for catalytic degradation kinetics have been calculated using the $\ln(C_o/C_t)$ slope against time. The values of k for CdS in the acidic, basic, and neutral media were calculated as 0.02173, 0.01417, and 0.00413 min^{-1}, respectively (Figure 11b).

The stability of the nanocatalyst was monitored in an acidic medium as CdS demonstrated sufficient degradation results; thus, its stability was studied by allowing the experiment to continue for 72 h to determine whether dye reduction in the presence of a nanocatalyst is stable or not. Therefore, the degraded dye was placed in the dark, and degradation was observed via absorption spectra recorded through a UV−vis spectrophotometer every 24 h. The results showed that no degradation loss occurred under stable conditions for 72 h, as shown in Figure 11c. Degradation was observed in its almost original form, confirming the catalyst's stability. A table of comparison of catalytic activity of QDs reported with present study shown in (Table 1).

4. CONCLUSIONS

The hydrothermal route has been used to synthesize cadmium sulfide (CdS) with an increasing concentration of Ba (3 and 6%) as a doped material. The CdS exhibits a crystalline nature with a hexagonal crystal structure, and the crystallite size decreased (20.73−18.73 nm). The surface and structure morphologies were confirmed through FE-SEM and TEM analyses, exhibiting agglomerated QDs for pure and Ba-doped samples. The elemental composition confirmed through EDS analysis showed the presence of Cd and S for pure and Ba elements for all doped samples. The interlayer d-spacings of pure and Ba (3 and 6%) doped CdS were measured as 0.35, 0.20, and 0.24 nm, respectively. It was shown to have catalytic activity for the degradation of the MB dye in the presence of $NaBH_4$, and the findings showed that it could degrade the MB dye up to 62.59% in neutral, 72.74% in acidic, and 71.33% in basic mediums. The densities of states of the pure and doped CdS surface were computed to examine the impact of Ba doping on the CdS surface from the perspective of electronic structures. The band-gap values appear to be slightly decreasing with rising Ba concentrations. The absorption spectrum research revealed that the pure and doped CdS absorbed photons in the visible range. This study degraded the methylene blue dye and evaluated DFT.

■ ASSOCIATED CONTENT

Supporting Information

The Supporting Information is available free of charge at https://pubs.acs.org/doi/10.1021/acsomega.2c04862.

Figure S1, FE-SEM images with low and high magnification; Figure S2, time-dependent UV−vis absorption spectra in an acidic medium for reduction of MB (PDF)

https://doi.org/10.1021/acsomega.2c04862
ACS Omega 2022, 7, 46325−46336

AUTHOR INFORMATION

Corresponding Authors

Muhammad Ikram − *Solar Cell Applications Research Lab, Department of Physics, Government College University Lahore, Lahore 54000 Punjab, Pakistan;* orcid.org/0000-0001-7741-789X; Email: dr.muhammadikram@gcu.edu.pk

Walid Nabgan − *Departament d'Enginyeria Química, Universitat Rovira i Virgili, 43007 Tarragona, Spain;* Email: walid.nabgan@urv.cat

Authors

Ata Ur Rehman − *Solar Cell Applications Research Lab, Department of Physics, Government College University Lahore, Lahore 54000 Punjab, Pakistan*

Ali Haider − *Department of Clinical Sciences, Faculty of Veterinary and Animal Sciences, Muhammad Nawaz Shareef University of Agriculture (MNSUA), Multan 66000, Pakistan*

Muhammad Asif Raza − *Department of Clinical Sciences, Faculty of Veterinary and Animal Sciences, Muhammad Nawaz Shareef University of Agriculture (MNSUA), Multan 66000, Pakistan*

Tahira Shujah − *Department of Physics, University of Central Punjab, Lahore 54000, Pakistan*

Misbah Naz − *Department of Chemistry, Division of Science and Technology, University of Education, Lahore, Punjab 54000, Pakistan*

Anwar Ul-Hamid − *Center for Engineering Research, Research Institute, King Fahd University of Petroleum & Minerals, Dhahran 31261, Saudi Arabia;* orcid.org/0000-0002-0259-301X

Iram Shahzadi − *Punjab University College of Pharmacy, University of the Punjab, Lahore, Punjab 54000, Pakistan*

Souraya Goumri-Said − *College of Science, Physics Department, Alfaisal University, Riyadh 11533, Saudi Arabia;* orcid.org/0000-0002-9333-7862

Mohammed Benali Kanoun − *Department of Mathematics and Sciences, College of Humanities and Sciences, Prince Sultan University, Riyadh 11586, Saudi Arabia*

Complete contact information is available at: https://pubs.acs.org/10.1021/acsomega.2c04862

Notes

The authors declare no competing financial interest.

ACKNOWLEDGMENTS

The authors would like to express their gratitude to HEC, who provided financial support via NRPU-20-17615 (Dr. Muhammad Ikram), Pakistan.

REFERENCES

(1) United Nations. *Executive Summary: Water for a Sustainable World*, The United Nations World Water Development Report, 2015.

(2) Fernández, C.; Larrechi, M. S.; Callao, M. P. An Analytical Overview of Processes for Removing Organic Dyes from Wastewater Effluents. *TrAC, Trends Anal. Chem.* **2010**, *29*, 1202−1211.

(3) Manikandan, B.; Ramamurthi, V.; Karthikeyan, R.; Sundararaman, T. R. Biobleaching of Textile Dye Effluent Using Mixed Culture through an Immobilized Packed Bed Bio Reactor (IPBBR). *Mod. Appl. Sci.* **2009**, *3*, 131−135.

(4) Chowdhury, S.; Saha, P. Adsorption Kinetic Modeling of Safranin onto Rice Husk Biomatrix Using Pseudo-First- and Pseudo-Second-Order Kinetic Models: Comparison of Linear and Non-Linear Methods. *Clean: Soil, Air, Water* **2011**, *39*, 274−282.

(5) Al-Degs, Y. S.; El-Barghouthi, M. I.; El-Sheikh, A. H.; Walker, G. M. Effect of Solution PH, Ionic Strength, and Temperature on Adsorption Behavior of Reactive Dyes on Activated Carbon. *Dyes Pigm.* **2008**, *77*, 16−23.

(6) Al-Kdasi, A.; Idris, A.; Saed, K.; Guan, C. T. Treatment of Textile Wastewater by Advanced Oxidation Processes− A Review. *Global NEST J.* **2004**, *6*, 222−230.

(7) Sartape, A. S.; Mandhare, A. M.; Jadhav, V. V.; Raut, P. D.; Anuse, M. A.; Kolekar, S. S. Removal of Malachite Green Dye from Aqueous Solution with Adsorption Technique Using Limonia Acidissima (Wood Apple) Shell as Low Cost Adsorbent. *Arabian J. Chem.* **2017**, *10*, S3229−S3238.

(8) Hajati, S.; Ghaedi, M.; Mahmoudi, Z.; Sahraei, R. SnO2 Nanoparticle-Loaded Activated Carbon for Simultaneous Removal of Acid Yellow 41 and Sunset Yellow; Derivative Spectrophotometric, Artificial Neural Network and Optimization Approach. *Spectrochim. Acta, Part A* **2015**, *150*, 1002−1012.

(9) Kriegel, I.; Jiang, C.; Rodríguez-Fernández, J.; Schaller, R. D.; Talapin, D. V.; Da Como, E.; Feldmann, J. Tuning the Excitonic and Plasmonic Properties of Copper Chalcogenide Nanocrystals. *J. Am. Chem. Soc.* **2012**, *134*, 1583−1590.

(10) Kundu, J.; Pradhan, D. Controlled Synthesis and Catalytic Activity of Copper Sulfide Nanostructured Assemblies with Different Morphologies. *ACS Appl. Mater. Interfaces* **2014**, *6*, 1823−1834.

(11) Xu, X.; Zhai, T.; Shao, M.; Huang, J. Anodic Formation of Anatase TiO 2 Nanotubes with Rod-Formed Walls for Photocatalysis and Field Emitters. *Phys. Chem. Chem. Phys.* **2012**, *14*, 16371−16376.

(12) Panda, N.; Sahoo, H.; Mohapatra, S. Decolourization of Methyl Orange Using Fenton-like Mesoporous Fe2O3-SiO2 Composite. *J. Hazard. Mater.* **2011**, *185*, 359−365.

(13) TiO 2−Multi-Walled Carbon Nanotube Nanocomposites: Hydrothermal Synthesis and Temporally-Dependent Optical Properties. pubs.rsc.org.

(14) Sivakumar, M.; Towata, A.; Yasui, K.; Tuziuti, T.; Kozuka, T.; Iida, Y. Dependence of Sonochemical Parameters on the Platinization of Rutile Titania - An Observation of a Pronounced Increase in Photocatalytic Efficiencies. *Ultrason. Sonochem.* **2010**, *17*, 621−627.

(15) Shukla, J.; Mishra, A. Influence of Ba2+ Doping on Structural and Electrical Transport Properties of YMnO3 Ceramics. *J. Supercond. Novel Magn.* **2021**, *34*, 451−459.

(16) Park, J. C.; Kim, J.; Kwon, H.; Song, H. Gram-Scale Synthesis of Cu2O Nanocubes and Subsequent Oxidation to CuO Hollow Nanostructures for Lithium-Ion Battery Anode Materials. *Adv. Mater.* **2009**, *21*, 803−807.

(17) Rafiq, A.; Imran, M.; Ikram, M.; Naz, M.; Aqeel, M.; Majeed, H.; Hussain, S. G.; Ali, S. Photocatalytic and Catalytic Degradation of Organic Dye by Uncapped and Capped ZnS Quantum Dots. *Mater. Res. Express* **2019**, *6*, No. 055801.

(18) Fu, K.; Huang, J.; Yao, N.; Xu, X.; Wei, M. Enhanced Photocatalytic Activity Based on Composite Structure with Down-conversion Material and Graphene. *Ind. Eng. Chem. Res.* **2016**, *55*, 1559−1565.

(19) Fu, K.; Huang, J.; Yao, N.; Xu, X.; Wei, M. Enhanced Photocatalytic Activity of TiO2 Nanorod Arrays Decorated with CdSe Using an Upconversion TiO2:Yb3+,Er3+ Thin Film. *Ind. Eng. Chem. Res.* **2015**, *54*, 659−665.

(20) Wan, X.; Liang, X.; Zhang, C.; Li, X.; Liang, W.; Xu, H.; Lan, S.; Tie, S. Morphology Controlled Syntheses of Cu-Doped ZnO, Tubular Zn(Cu)O and Ag Decorated Tubular Zn(Cu)O Microcrystals for Photocatalysis. *Chem. Eng. J.* **2015**, *272*, 58−68.

(21) Rafiq, A.; Imran, M.; Aqeel, M.; Naz, M.; Ikram, M.; Ali, S. Study of Transition Metal Ion Doped CdS Nanoparticles for Removal of Dye from Textile Wastewater. *J. Inorg. Organomet. Polym. Mater.* **2020**, *30*, 1915−1923.

(22) Morales-Acevedo, A. Can We Improve the Record Efficiency of CdS/CdTe Solar Cells? *Sol. Energy Mater. Sol. Cells* **2006**, *90*, 2213−2220.

(23) Fard, N. E.; Fazaeli, R.; Ghiasi, R. Band Gap Energies and Photocatalytic Properties of CdS and Ag/CdS Nanoparticles for Azo Dye Degradation. *Chem. Eng. Technol.* **2016**, *39*, 149−157.
(24) Chauhan, R.; Kumar, A.; Chaudhary, R. P. Photocatalytic Degradation of Methylene Blue with Fe Doped ZnS Nanoparticles. *Spectrochim. Acta, Part A* **2013**, *113*, 250−256.
(25) Pande, C. B.; Moharir, K. N.; Khadri, S. F. R.; Patil, S. Study of Land Use Classification in an Arid Region Using Multispectral Satellite Images. *Appl. Water Sci.* **2018**, *8*, No. 123.
(26) Dabhane, H.; Ghotekar, S.; Tambade, P.; et al. A Review on Environmentally Benevolent Synthesis of CdS Nanoparticle and Their Applications. *Environ. Chem. Ecotoxicol.* **2021**, *3*, 209−219.
(27) Yaseen, M.; Ambreen, H.; Zia, M.; Javed, H. M. A.; Mahmood, A.; Murtaza, A. Study of Half Metallic Ferromagnetism and Optical Properties of Mn-Doped CdS. *J. Supercond. Nov. Magn.* **2021**, *34*, 135−141.
(28) Munyai, S.; Hintsho-Mbita, N. C. Green Derived Metal Sulphides as Photocatalysts for Waste Water Treatment. A Review. *Curr. Res. Green Sustainable Chem.* **2021**, *4*, No. 100163.
(29) Freitas, J. N.; Gonçalves, A. S.; Nogueira, A. F. A Comprehensive Review of the Application of Chalcogenide Nanoparticles in Polymer Solar Cells. *Nanoscale* **2014**, *6*, 6371−6397.
(30) Heo, K.; Lee, H.; Park, Y.; Park, J.; Lim, H. J.; Yoon, D.; Lee, C.; Kim, M.; Cheong, H.; Park, J.; Jian, J.; Hong, S. Aligned Networks of Cadmium Sulfide Nanowires for Highly Flexible Photodetectors with Improved Photoconductive Responses. *J. Mater. Chem.* **2012**, *22*, 2173−2179.
(31) Navale, S. T.; Mane, A. T.; Chougule, M. A.; Shinde, N. M.; Kim, J.; Patil, V. B. Highly Selective and Sensitive CdS Thin Film Sensors for Detection of NO2 Gas. *RSC Adv.* **2014**, *4*, 44547−44554.
(32) Abd-Elkader, O. H.; Shaltout, A. A. Characterization and Antibacterial Capabilities of Nanocrystalline CdS Thin Films Prepared by Chemical Bath Deposition. *Mater. Sci. Semicond. Process.* **2015**, *35*, 132−138.
(33) Rathore, K. S.; Deepika; Patidar, D.; Saxena, N. S.; Sharma, K. Cadmium Sulphide Nanocrystallites: Synthesis, Optical and Electrical Studies. *AIP Conf. Proc.* **2010**, *1249*, 145−148.
(34) Salavati-Niasari, M.; Loghman-Estarki, M. R.; Davar, F. Controllable Synthesis of Nanocrystalline CdS with Different Morphologies by Hydrothermal Process in the Presence of Thioglycolic Acid. *Chem. Eng. J.* **2008**, *145*, 346−350.
(35) Sivaraman, T.; Nagarethinam, V. S.; Balu, A. R.; Usharani, K. Structural, Morphological, Optical and Electrical Properties of CdS Thin Fils Simultaneously Doped with Magnesium and Chlorine. *J. Mater. Sci.: Mater. Electron.* **2016**, *27*, 1158−1164.
(36) Priyadharsini, N.; Elango, M.; Vairam, S.; Thamilselvan, M. Effect of Nickel Substitution on Structural, Optical, Magnetic Properties and Photocatalytic Activity of ZnS Nanoparticles. *Mater. Sci. Semicond. Process.* **2016**, *49*, 68−75.
(37) Banumathi, M. T. V.; Nirmala, M. B.PROJECT DETAILS-Department of Physics-III UG. gvgvc.ac.in.
(38) Susha, N.; Nandakumar, K.; Nair, S. R. Enhanced Photoconductivity in CdS/Betanin Composite Nanostructures. *RSC Adv.* **2018**, *8*, 11330−11337.
(39) Tripathi, R. M.; Bhadwal, A. S.; Singh, P.; Shrivastav, A.; Singh, M. P.; Shrivastav, B. R. Mechanistic Aspects of Biogenic Synthesis of CdS Nanoparticles Using Bacillus Licheniformis. *Adv. Nat. Sci. Nanosci. Nanotechnol.* **2014**, *5*, No. 025006.
(40) Sabah, A.; Siddiqi, S. A.; Ali, S. Fabrication and Characterization of CdS Nanoparticles Annealed by Using Different Radiations. *World Acad. Sci. Eng. Technol.* **2010**, *70*, 82−89.
(41) Devadoss, I.; Sakthivel, P.; Krishnamoorthy, A. Band Gap Tailoring and Photoluminescence Performance of CdS Quantum Dots for White LED Applications: Influence of Ba2+ and Zn2+ Ions. *J. Mater. Sci. Mater. Electron.* **2021**, *32*, 5729−5737.
(42) Ikram, M.; Abid, N.; Haider, A.; Ul-Hamid, A.; Haider, J.; Shahzadi, A.; Nabgan, W.; Goumri-Said, S.; Butt, A. R.; Benali Kanoun, M. Toward Efficient Dye Degradation and the Bactericidal Behavior of Mo-Doped La2O3nanostructures. *Nanoscale Adv.* **2022**, *4*, 926−942.
(43) Chandekar, K.; Shkir, M.; Khan, A.; AlFaify, S. An In-Depth Study on Physical Properties of Facilely Synthesized Dy@ CdS NPs through Microwave Route for Optoelectronic Technology. *Mater. Sci. Semicond. Process.* **2020**, *118*, No. 105184.
(44) Samiyammal, P.; Parasuraman, K.; Balu, A. R. (Ba+Co) Codoped CdS Thin Films with Enhanced Magnetic and Photodegradation Properties. *Mater. Res. Express* **2019**, *6*, No. 056414.
(45) Dey, P. C.; Das, R. Photoluminescence Quenching in Ligand Free CdS Nanocrystals Due to Silver Doping along with Two High Energy Surface States Emission. *J. Lumin.* **2017**, *183*, 368−376.
(46) Gonzalez, M.; Marquez, A.; Zapata, M.et al.Cadmium Sulfide Pellets for Growth of Thin Films By Pulsed Laser Deposition. 2007, pp 1−10.
(47) Kotkata, M. F.; Masoud, A. E.; Mohamed, M. B.; Mahmoud, E. A. Synthesis and Structural Characterization of CdS Nanoparticles. *Phys. E* **2009**, *41*, 1457−1465.
(48) Smidstrup, S.; Markussen, T.; Vancraeyveld, P.; Wellendorff, J.; Schneider, J.; Gunst, T.; Verstichel, B.; Stradi, D.; Khomyakov, P. A.; Vej-Hansen, U. G.; Lee, M. E.; Chill, S. T.; Rasmussen, F.; Penazzi, G.; Corsetti, F.; Ojanperä, A.; Jensen, K.; Palsgaard, M. L. N.; Martinez, U.; Blom, A.; Brandbyge, M.; Stokbro, K. QuantumATK: An Integrated Platform of Electronic and Atomic-Scale Modelling Tools. *J. Phys. Condens. Matter* **2020**, *32*, No. 015901.
(49) Perdew, J. P.; Burke, K.; Ernzerhof, M. Generalized Gradient Approximation Made Simple. *Phys. Rev. Lett.* **1996**, *77*, 3865−3868.
(50) Ferreira, L. G.; Marques, M.; Teles, L. K. Approximation to Density Functional Theory for the Calculation of Band Gaps of Semiconductors. *Phys. Rev. B: Condens. Matter Mater. Phys.* **2008**, *78*, No. 125116.
(51) Kanoun, M. B.; Goumri-Said, S.; Schwingenschlögl, U.; Manchon, A. Magnetism in Sc-Doped ZnO with Zinc Vacancies: A Hybrid Density Functional and GGA + U Approaches. *Chem. Phys. Lett.* **2012**, *532*, 96−99.
(52) Kaur, K.; Lotey, G. S.; Verma, N. K. Ferromagnetism in Gd-Doped CdS Dilute Magnetic Semiconducting Nanorods. *J. Mater. Sci. Mater. Electron.* **2014**, *25*, 311−316.
(53) Kanoun, M. B. Insight into the Origin of Magnetism in Iron-Doped Cadmium Sulfide Thin Films from First Principles Calculations. *Solid State Commun.* **2017**, *253*, 10−13.
(54) Biswas, A.; Meher, S. R.; Kaushik, D. K. Electronic and Band Structure Calculation of Wurtzite CdS Using GGA and GGA+*U* Functionals. *J. Phys.: Conf. Ser.* **2022**, *2267*, No. 12155.
(55) Soltani, N.; Gharibshahi, E.; Saion, E. Band Gap of Cubic and Hexagonal Cds Quantum Dots-Experimental and Theoretical Studies. *Chalcogenide Letters* **2012**, 321−328.
(56) Hassan, J.; Naz, S.; Haider, A.; Raza, A.; Ul-Hamid, A.; Qumar, U.; Haider, J.; Goumri-Said, S.; Kanoun, M. B.; Ikram, M. H-BN Nanosheets Doped with Transition Metals for Environmental Remediation; a DFT Approach and Molecular Docking Analysis. *Mater. Sci. Eng., B* **2021**, *272*, No. 115365.
(57) Shaheen, S.; Iqbal, A.; Ikram, M.; Ul-Ain, K.; Naz, S.; Ul-Hamid, A.; Shahzadi, A.; Haider, A.; Nabgan, W.; Haider, J. Effective Disposal of Methylene Blue and Bactericidal Benefits of Using GO-Doped MnO2Nanorods Synthesized through One-Pot Synthesis. *ACS Omega* **2021**, *6*, 24866−24878.
(58) Ikram, M.; Abbas, S.; Haider, A.; Naz, S.; Ahmad, S. O. A.; Haider, J.; Ul-Hamid, A.; Shahzadi, A.; Shahzadi, I.; Butt, A. R. Efficient Dye Degradation, Antimicrobial Behavior and Molecular Docking Analysis of Gold (Au) and Cellulose Nanocrystals (CNC)-Doped Strontium Oxide Nanocomposites. *J. Nanostructure Chem.* **2021**, 933.
(59) Ikram, M.; Tabassum, R.; Qumar, U.; Ali, S.; Ul-Hamid, A.; Haider, A.; Raza, A.; Imran, M.; Ali, S. Promising Performance of Chemically Exfoliated Zr-Doped MoS2nanosheets for Catalytic and Antibacterial Applications. *RSC Adv.* **2020**, *10*, 20559−20571.
(60) Rafique, A.; Ikram, M.; Haider, A.; Ul-Hamid, A.; Naz, S.; Nabgan, W.; Haider, J.; Shahzadi, I. Dye Degradation, Antibacterial

https://doi.org/10.1021/acsomega.2c04862
ACS Omega 2022, 7, 46325−46336

Activity and Molecular Docking Analysis of Cellulose/Polyvinylpyrrolidone-Doped Cadmium Sulphide Quantum Dots. *Int. J. Biol. Macromol.* **2022**, *214*, 264−277.
(61) Ikram, M.; Hayat, S.; Imran, M.; Haider, A.; Naz, S.; Ul-Hamid, A.; Shahzadi, I.; Haider, J.; Shahzadi, A.; Nabgan, W.; Ali, S. Novel Ag/Cellulose-Doped CeO2 Quantum Dots for Efficient Dye Degradation and Bactericidal Activity with Molecular Docking Study. *Carbohydr. Polym.* **2021**, *269*, No. 118346.
(62) Junaid, M.; Imran, M.; Ikram, M.; Naz, M.; Aqeel, M.; Afzal, H.; Majeed, H.; Ali, S. The Study of Fe-Doped CdS Nanoparticle-Assisted Photocatalytic Degradation of Organic Dye in Wastewater. *Appl. Nanosci.* **2019**, *9*, 1593−1602.

https://doi.org/10.1021/acsomega.2c04862
ACS Omega 2022, 7, 46325−46336